THE JOURNAL OF PHYSICAL CHEMISTRY C
A JOURNAL OF THE AMERICAN CHEMICAL SOCIETY

pubs.acs.org/JPCC

Article

Ultrafast Transient Absorption Spectroscopy of Inkjet-Printed Graphene and Aerosol Gel Graphene Films: Effect of Oxygen and Morphology on Carrier Relaxation Dynamics

Alexander J. Auty,* Negar Mansouriboroujeni, Thiba Nagaraja, Dimitri Chekulaev, Christopher M. Sorensen, Suprem R. Das, Natalia Martsinovich, and Adrien A. P. Chauvet*

Cite This: J. Phys. Chem. C 2022, 126, 7949−7955

Read Online

ACCESS | Metrics & More | Article Recommendations | Supporting Information

ABSTRACT: The tunable electronic properties of nanostructured graphene make it one of the most sought alternatives to metals for novel technological applications. In particular, the ability to prepare inks out of these nanostructures allows for printable and thus scalable graphene-based electronics. Here, we investigate the electronic properties of novel inkjet-printed aerosol gel graphene (AG) films and compare them to those of inkjet-printed graphene (G) films. More specifically, we report on the photoinduced carrier dynamics of these materials via ultrafast transient absorption spectroscopy. In comparison to graphene, AG films have a higher oxygen content as well as a complex 3D morphology. While G and AG both differ in composition and structure, the similitude in their carrier−optical phonon scatter rates (in 74−140 fs range) indicates a comparable lattice defect density. It is therefore not the number of defects but the type of defect that is electronically relevant. Indeed, in comparison to G films, which exhibit complete recovery of the transient signal, the AG films exhibit only partial recovery within our 400 ps experimental time window. The persisting signal is assigned to trapped electronic states. These long-lived electronic states are most probably due to the presence of oxygen rather than due to the films' unique 3D morphology.

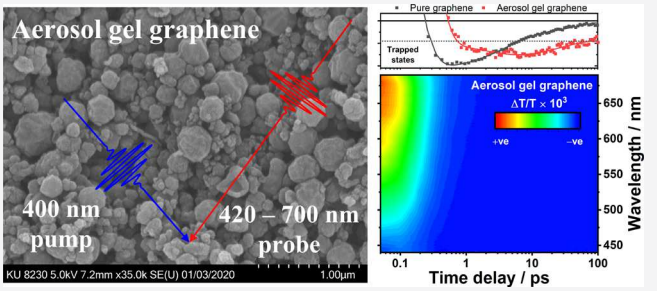

1. INTRODUCTION

The unique two-dimensional honeycomb structure of graphene gives rise to equally unique electronic and optical properties. Graphene is a zero-band gap semiconductor with a linear energy dispersion curve and as such, the band structure is often represented as two cones touching at the Dirac point, as depicted in Figure 1.[1,2] Given graphene's unique mechanical and electronic properties, many have proposed to use it in various applications ranging from ultrafast electronic devices to chemical sensors.[1−5] In most cases, the performance of such applications is dependent on the carrier dynamics [e.g., carrier−carrier (C−C) and carrier−phonon scattering], especially carriers at energies well above the ambient lattice temperature. For example, in some devices the charge transport is determined by the transient conductivity of hot carriers, well above the Fermi level. Therefore, understanding the relaxation of hot carriers is of paramount importance for device development.[6] However, such carrier dynamics takes place on ultrafast time scales: in the femto- to picosecond range. Accordingly, ultrafast spectroscopy is best suited to investigate the photoinduced carrier dynamics that are relevant to graphene's performances.[7−9] Dawlaty et al. pioneered using degenerate pump−probe spectroscopy to measure the carrier relaxation dynamics in epitaxial graphene.[10] Epitaxial graphene

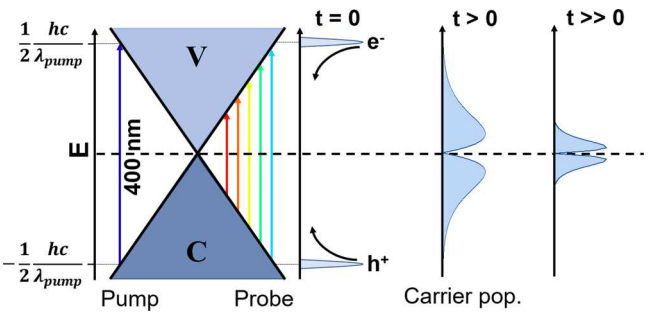

Figure 1. (Left) Band structure of graphene, with the colored arrows depicting the interaction of the pump and the probe laser pulses with the electronic structure of graphene. (Right) Evolution of the carrier (electron and hole) populations as a function of pump−probe delay, *t*, and energy, *E*.

Received: February 14, 2022
Revised: March 30, 2022
Published: April 20, 2022

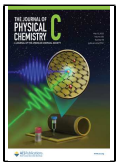

https://doi.org/10.1021/acs.jpcc.2c01086
J. Phys. Chem. C 2022, 126, 7949−7955

was shown to exhibit lifetimes of 70−120 fs for C−C scattering and 0.4−1.7 ps for carrier−optical phonon (C−OP) scattering. With the aim of tuning graphene's electronic properties, various graphene-based materials have been produced and characterized via ultrafast spectroscopy. One of the most promising materials for large-scale applications such as energy storage devices and sensors is graphene with a highly crumpled structure.[11−14] The carrier dynamics of this type of graphene aerosol gel is, however, lacking understanding. We therefore propose to address the gap of knowledge by investigating this novel and promising material via ultrafast pump−probe spectroscopy.

In this work, we thus report the first ultrafast pump−probe spectroscopic study of aerosol gel graphene (AG) films. This study focuses on photoinduced carrier dynamics and complements the previously reported chemical and morphological characterization of AG inks.[11] In the latter work, the authors emphasized the significant structural differences between standard graphene ink and AG ink. More specifically, it was shown that, while typical graphene ink corresponds to a suspension of 2D graphene flakes, the AG ink contains a mixture of quasi-3D (crumpled 2D flakes) and 2D graphene flakes, as shown in Figure 2. In addition to the differing

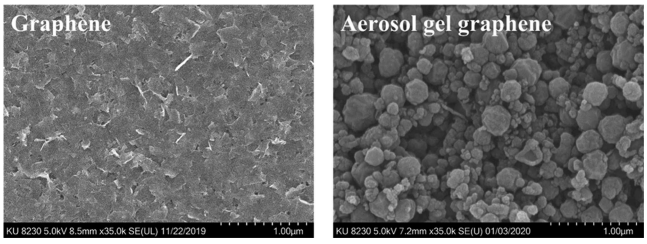

Figure 2. Scanning electron microscopy images of representative samples of graphene ink flakes (left) and AG ink flakes (right).

morphology, the AG ink is also found to have a higher oxygen content.[11] Therefore, the present study aims at distinguishing which of the two, changes in morphology or oxygen content, is most affecting the graphene's carrier dynamics.

The carrier dynamics are here investigated by means of ultrafast spectroscopy in the transmission mode. The transmission of light through graphene is generally determined by the interband absorption (Figure 1). Interband absorption is proportional to the carrier occupation probability in the conduction band (c), $f_c(E)$, and the valence band (v), $f_v(E)$, at a given energy, E, above and below the Dirac point.[6] The carrier occupation is determined by the Fermi function and the density of states, which is a linear dispersion function for pure graphene. Excitation with a pump pulse of wavelength, λ_p, will produce a nonequilibrium distribution of carriers at an energy of $hc/2\lambda_p$, above and below the Dirac point (Figure 1). These carriers will first thermalize through ultrafast C−C scattering, with rates reported between 0.2 and 40 fs.[15,16] Given the sub 40 fs nature of C−C scattering, we are not expecting to monitor carrier thermalization because it falls below our ∼100 fs time resolution. However, we do expect to monitor all of the subsequent carrier cooling, via C−OP scattering, lattice cooling, trapped state formation, and final charge recombination.

2. EXPERIMENTAL METHODS

2.1. Preparation of the Graphene and Oxygen-Containing Aerosol Gel Graphene Films. The graphene ink was synthesized from graphite powders (Millipore Sigma) using a slightly modified protocol. In brief, pure graphene ink was synthesized with a high shear force using graphite powder (Millipore Sigma). A similar strategy was followed to synthesize AG ink, but the starting material was produced following a gas phase hydrocarbon and oxygen co-detonation process.[11] The graphene and AG inks were inkjet-printed as a 0.5 by 0.5 square centimeter pattern, onto quartz substrates, each with three different thicknesses, referred to as G1, G2, and G3 and AG1, AG2, and AG3, respectively. The numbering refers to the number of printing passes. Accordingly, the films thicknesses increase from 1 to 3.

2.2. UV−Vis Spectroscopy. UV−vis absorption measurements were taken using an Agilent Cary 60 UV−vis spectrometer.

2.3. Pump−Probe Spectroscopy. UV−vis pump−probe spectroscopy experiments were performed in the Lord Porter Ultrafast Laser Laboratory (ULS), The University of Sheffield, using a Helios system (HE-VIS-NIR-3200) provided by Ultrafast Systems. A Ti:sapphire regenerative amplifier (Spitfire Ace PA-40, Spectra-Physics) provides 800 nm pulses (40 fs full width at half-maximum, 10 kHz, 1.2 μJ). The 400 nm pump pulses (2.5 kHz, 0.2 μJ) were generated through frequency doubling of the amplifier fundamental. The pump was focused onto the sample film to a beam diameter of approximately 275 μm. The white light probe continuum (440−700 nm) was generated using a sapphire crystal and a portion of the amplifier fundamental. The intensity of the probe light transmitted through the sample was measured using a CMOS camera, with a resolution of 1.5 nm. Prior to generation of the white light, the 800 nm pulses were passed through a computer-controlled optical delay line (DDS300, Thorlabs), which provides up to 8 ns of pump−probe delay. The instrument response function is approximately 100 fs based on the temporal duration of the coherent artifact signal from the quartz substrate. All steady state and time-resolved spectroscopic data were processed using OriginPro. Preprocessing of the pump−probe data was performed using Surface Xplorer, the software package provided by Ultrafast Systems. Kinetic traces from the pump−probe data were fit in OriginPro using a sum of decaying exponential functions convoluted with a Gaussian function. The Gaussian function was used to model the instrument response growth of the transient signal. The function can be found in the Supporting Information.

2.4. Theoretical Calculations. Simulations of the UV−vis absorption spectra of graphene and graphene doped with oxygen were performed using SIESTA software. Modeling details can be found in the Supporting Information.

3. RESULTS AND DISCUSSION

The steady-state optical transmission of the graphene and AG films is shown in Figure 3, for three different film thicknesses (1, 2, and 3 printing passes). In addition, steady-state Raman spectra of representative graphene and AG inks are given in Supporting Information, Figure S1. As previously reported, graphene films are characterized by broad absorption between 200 and 800 nm, with a minimum in the transmission spectrum at 267 nm.[17−19] Based on this literature, the peak is assigned to a $\pi \rightarrow \pi^*$ electronic transition of the graphene. The

https://doi.org/10.1021/acs.jpcc.2c01086
J. Phys. Chem. C 2022, 126, 7949−7955

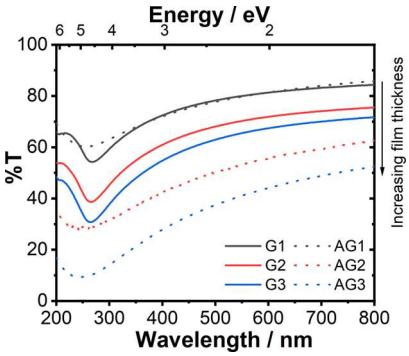

Figure 3. UV−vis transmission spectra of graphene films (G, solid) and aerogel graphene films (AG, dashed) printed on quartz.

AG films also display broad absorption over the same spectral region. However, the minimum in the transmission spectrum is broadened and blue-shifted to ∼247 nm.

A similar blue shift in the $\pi \rightarrow \pi^*$ peak of graphene oxide relative to the same peak in reduced graphene oxide was already reported.[18] In addition, our density functional theory calculations of the ground-state electronic absorption spectrum graphene doped with oxygen shows a broadening of the $\pi \rightarrow \pi^*$ peak, when compared to the calculated spectrum of pure graphene (see Supporting Information, Figure S2). Similar modeling of bent graphene sheet also shows broadening of the ground-state electronic absorption spectrum with its peak shifted to the red. Accordingly, while the broadening could be the result of both, the presence of oxygen and the unique 3D structure of AG, the blue-shifted UV−vis spectra is a signature for the presence of oxygen. As illustrated by Table 1, the

Table 1. % *T* Values and the Estimated Number of Layers for the G and AG Films

films	% *T* (800 nm)	no. of layers[a]
G1	84.4	7
G2	75.6	12
G3	71.6	14
AG1	85.9	7
AG2	62.6	20
AG3	52.4	28

[a]The number of layers is derived from each sample's absorption at 800 nm.

progressive increase in film thickness results in the reduction of the transmission of the incident light. Assuming that one layer of graphene absorbs 2.3% of incident white light,[20] the approximate number of layers in the graphene and AG samples have been estimated and are given in Table 1.

The transient changes in transmission ($\Delta T/T$) of all the graphene and AG samples were measured, following excitation with a 400 nm laser pulse (0.2 μJ). The $\Delta T/T$ signal acquired from G3 and AG3 is shown in Figure 4. There was minimal dependence of the $\Delta T/T$ signal dynamics on the film thickness. Therefore, the transient data for G1, G2, AG1, and AG2 are not presented in the main text but can be found in the Supporting Information (see Figures S3−S6). Following excitation, all the films display a broad positive signal which rises within the instrument response, reaching maximum values at ∼40 fs. Because this rise time is constant across the probed

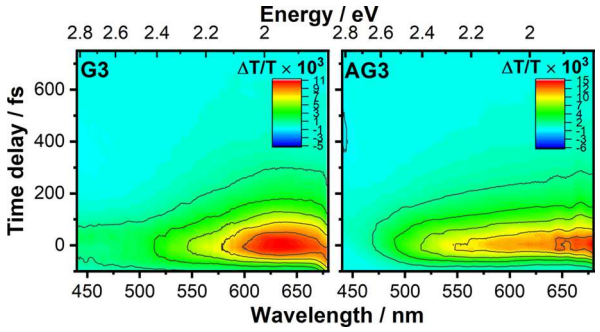

Figure 4. (Left) Change in transmission ($\Delta T/T$) of G3, following excitation at 400 nm, in the spectral range 440−680 nm, from −100 to 750 fs. (right) Change in transmission ($\Delta T/T$) of AG3, following excitation at 400 nm, in the spectral range 440−680 nm, from −100 to 750 fs.

range, it suggests that a hot carrier distribution is obtained within the instrument response (100 fs).

The initial positive signal is assigned to photobleaching of the broad ground-state absorption due to the depletion of the available valence to conduction band electronic transitions (i.e. Pauli blocking). Prompt loss of the initial signal is then observed for all the films. This behavior is exemplified by the kinetics traces of both G3 and AG3, as shown in Figure 5. In

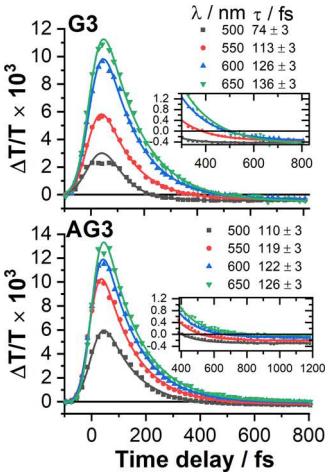

Figure 5. Single-point kinetic traces for G3 (top) and AG3 (bottom) overlaid with their exponential fits. The associated decay lifetimes are given alongside the wavelength in the legend.

the 50−500 fs time range, the decay of the initial bleach signal in the region from 500 to 650 nm, reveals decay lifetimes in the range of 74−136 fs for G3 and 110−126 fs for AG3. Similar loss of the initial positive $\Delta T/T$ signal of graphene films has already been previously reported.[10,15,21] Such a behavior has been attributed to cooling of the photogenerated carriers via C−C and C−OP scattering. Kinetic analysis reveals a linear increase in the extracted lifetime as the probe photon wavelength is increased (see Supporting Information, Figure S7). This demonstrates that carriers at higher energies lose their energy more rapidly compared to carriers with lesser energy and results from the increasing intraband C−OP scattering rate when the carrier energy increases.[22−24] Such a behavior suggests that the carrier scattering corresponds mainly to intervalley scattering with K and K' optical phonons.[24,25]

https://doi.org/10.1021/acs.jpcc.2c01086
J. Phys. Chem. C 2022, 126, 7949−7955

Defects have also been shown to play a significant role in the initial carrier cooling of graphene. In particular, defect-induced supercollision cooling provides the additional momentum needed to satisfy conservation restrictions.[26,27] This cooling involves the collision of a carrier with a defect and an acoustic phonon. An additional cooling pathway has been shown to increase the rate of initial carrier cooling in graphene, with the carrier cooling rate reported to have a linear dependence on defect density.[27] The similitude of C−OP scattering rates for G3 and AG3 thus suggest that the lattice defect density in both samples is similar.

The 500 fs to 1 ps time range is marked by a persisting negative signal for all samples, as shown in the insets of Figure 5. The negative signal present across the full probe spectral range (440−680 nm) corresponds to excited state absorption. Similar persisting (≫1 ps) negative $\Delta T/T$ signal for graphene films deposited on quartz has been previously reported.[14] The similar carrier dynamics and transient spectral features of inkjet-printed graphene ink (this work) with that of CVD-grown graphene, both deposited on quartz, suggests that the carrier dynamics are independent of the preparation technique. Negative $\Delta T/T$ signal could be ascribed to the shrinkage of the band separation (band gap renormalization), driven by the photogenerated hot carriers, which, in turn, are heating the lattice. Such a behavior has been observed both in graphene[15,24] and graphite samples.[25]

Negative $\Delta T/T$ signals, when probing with near-IR photon energies (1.5−2.6 μm), have also been attributed to a rise of the Fermi level in doped graphene layers.[6] However, while probing in the UV−vis range, we do not expect to monitor such small variations of the Fermi level. The kinetic behavior of the negative transmission signal, at 550 nm, is shown in Figure 6 for G3 and AG3. In the case of G3, the maximum negative

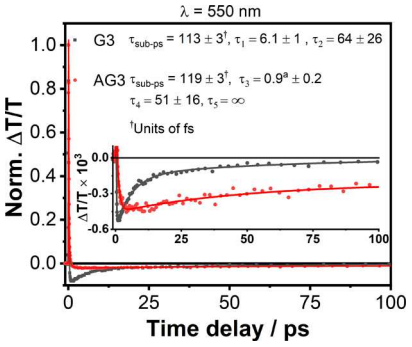

Figure 6. Kinetic traces at 550 nm for G3 and AG3. Inset corresponds to the expanded traces showing the negative recovery. The overlaid traces are the multiexponential fits, with the corresponding lifetimes (in ps) given in the legend. [a]Modeling the growth of the negative signal, not the recovery of the long-lived negative signal.

signal is reached at ∼770 fs, after which it decays biexponentially with lifetimes of 6.1 (τ_1) and 64 ps (τ_2). The decay component τ_2 is very similar to the previously monitored monoexponential recovery reported by Shang.[15] As will be discussed subsequently, the relative contributions of τ_1 and τ_2 to the recovery of the negative signal seem to be power-dependent and are both assigned to charge recombination and lattice cooling. In comparison to G3, the maximum negative signal for AG3 is reached at a pump−probe delay of 5 ps. The delay in reaching the maximum negative signal is reflected in the extraction of an additional lifetime of 0.9 ps, while fitting the growth of the negative $\Delta T/T$ signal. Clearly, the incorporation of oxygen into the graphene structure and/or the more complex three-dimensional (3D) structure of AG3 have a significant effect on the initial carrier dynamics. In AG3, about half of the negative signal decays with a lifetime of 51 ps, while the other half is non-decaying within the 400 ps time window of the experiment. Similar long-lived (≫1 ns) negative $\Delta T/T$ signal has been previously reported in graphene oxide suspended in water.[28] This signal was assigned by Kaniyankandy et al. to the presence of trapped states undergoing slow recombination. Via carrier quenching, the latter confirmed that the defect states mainly originated from oxygen sites, in the form of epoxides and carboxylic acid groups, which act as electron traps. The presence of a similar kinetic behavior suggests the possibility of similar trapped states in AG3, which are not present in G3. Therefore, the 0.9 ps lifetime may be indicative of "trapping" of the carriers by the oxygen sites. As previously alluded to, the AG inks also differ in flake morphology compared to the graphene inks, with the AG inks containing graphene flakes with a quasi-3D structure. The change in morphology cannot be discounted as a possible cause for the change in carrier dynamics observed. However, the AG films do not exhibit UV−vis transmission spectra that are typical of 3D nanostructured graphene materials such as nanotubes.[29] This suggests that the 3D-flakes have optical transmission properties more akin to that of planar graphene sheets. Although the recovery dynamics of graphene oxide and AG3 exhibit similarities, the late-time transmission spectra do not. It has been reported that the absorption of trapped carriers (at oxygen sites) in graphene oxide has a peak at 670 nm.[28] AG3 displays no such peak at later time delays. However, there is a distinct peak at approximately 520 nm in AG3's transient transmission spectrum. This contrasts with G3, where the later time-delay spectrum is flat in the region 440−680 nm, as shown in Figure 7. This behavior suggests that the nature of electronic states responsible for the negative signal at late times is different in G3 and AG3.

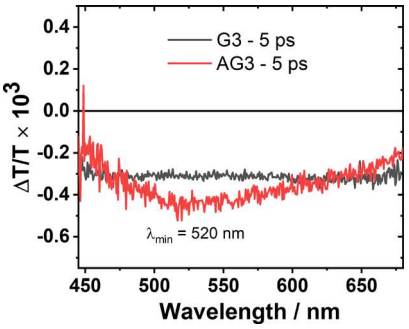

Figure 7. $\Delta T/T$ spectra of G3 and AG3 5 ps after excitation at 400 nm. The minimum of the spectrum for AG3 is labeled on the graph.

Pump energy (E_p) dependence of the kinetics at a probe wavelength of 550 nm is shown in Figure 8 for G3 and AG3. Multiexponential fittings reveal that the ultrafast, sub-ps, lifetime increases as E_p is increased, although the trend for the sub-ps lifetime of AG3 is weaker (see the "sub-ps lifetime" columns in the tables given in Figure 8). This results in the maximum negative signal being reached at later pump−probe time delays for G3, as E_p is increased (see the inset in top left graph of Figure 8). For G3, the growth of the negative signal is monoexponential for E_p = 0.02, 0.1, and 0.18 μJ, whereas this

https://doi.org/10.1021/acs.jpcc.2c01086
J. Phys. Chem. C 2022, 126, 7949−7955

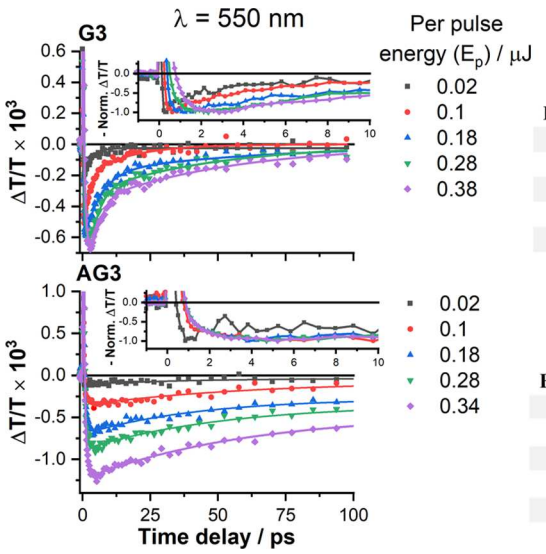

G3	Growth of negative signal		Recovery of negative signal				
E_p / μJ	Sub-ps τ / fs		τ_1 / ps	A_1	τ_2 / ps	A_2	A_1/A_2
0.02	47		1.9	0.76	45	0.16	4.9
0.1	100		2.1	0.83	15	0.30	2.8
0.18	114		4.6	0.80	50	0.30	2.7
	τ_a	τ_b					
0.28	125	2.2	3.6	0.90	36	0.46	1.9
0.38	138	1.7	3.9	0.88	43	0.50	1.8

AG3	Growth of negative signal		Recovery of negative signal			
E_p / μJ	Sub-ps τ / fs	τ_3 / ps	τ_4 / ps	$A_4^\dagger$	τ_5 / ps	$A_5^\dagger$
0.02	92	n/a	39	0.09	∞	0.08
0.1	117	0.5	61	0.36	∞	0.16
0.18	143	0.8	42	0.55	∞	0.59
0.28	129	0.6	51	0.69	∞	0.75
0.34	143	0.6	59	1	∞	1

Figure 8. (Left) Pump energy-dependent kinetics at 550 nm for both G3 (top) and AG3 (bottom). Five different energies are shown, ranging from 0.02 to 0.38 μJ, with the specific values given in the legend. (Right) Table showing the lifetimes obtained from multiexponential fittings of the kinetics traces. †Amplitudes normalized to the maximum amplitude.

growth is best fit with two exponential functions (τ_a and τ_b) for E_p = 0.28 and 0.38 μJ. This signal dependence indicates that the nature of the initial carrier relaxation mechanism changes as E_p increases. A possible explanation for this behavior is the presence of a hot optical phonon bottleneck at higher pump energies. Following excitation, the hot carriers will lose most of their energy to the formation of hot optical phonons via sequential C−OP scattering events.[23] The main optical phonon modes responsible for the energy dissipation are the intravalley (Γ) and intervalley (K) optical phonons, K-A_1', Γ-$E_{2g,LO}$, and Γ-$E_{2g,TO}$, where LO and TO are longitudinal and transverse optical phonons, respectively.[22]

Subsequent cooling of the carriers is then coupled to the cooling of the hot optical phonons and as such, τ_b may reflect the cooling rate of the hot optical phonons. At lower values of E_p, and therefore, at lower carrier densities, it is possible that the role of a hot phonon bottleneck in the carrier relaxation dynamics is negligible. Conversely, the pump−probe time delay at which the maximum negative signal is reached in AG3 seems independent of E_p (except for the 0.02 μJ trace, which is deemed unreliable due to the very low S/N level). We do not observe any obvious trend in the G3 recovery lifetimes τ_1 and τ_2, as E_p is increased. However, the ratio of the τ_1 and τ_2 preexponential factors (amplitude A_1 and A_2, respectively) steadily decreases from 4.9 to 1.8, when E_p increases from 0.02 to 0.38 μJ. With regards to AG3, the recovery kinetics (τ_4 and τ_5) also appear to be independent of E_p. If, as it is expected, the slowly recombining trapped carriers are responsible for the negative signal at late-time (>400 ps), then the signal is also expected to saturate at higher values of E_p. However, no saturation is observed, with the amplitude of the non-decaying signal increasing linearly with E_p (see the A_5 column given of the table given in Figure 8). It is possible that the maximum pump energy reached in these experiments was insufficient to observe such a behavior.

4. CONCLUSIONS

The carrier relaxation dynamics of inkjet-printed graphene and AG films were investigated by means of ultrafast UV−vis pump−probe spectroscopy. These dynamics were here independent of the film's thickness. Similar ultrafast C−OP scattering lifetimes were observed for G3 (74−136 fs) and AG3 (110−126 fs), indicating that the lattice defect density in the novel aerosol gel ink is comparable to that of pure graphene ink. The C−OP scattering rates of the G and AG films showed a linear dependence on the probe photon energy. Following the ultrafast C−OP scattering, the G films display a negative $\Delta T/T$ signal, which recovers biexponentially (for G3, τ_1 = 6.1 and τ_2 = 64 ps at λ = 550 nm). The kinetic recovery is assigned to the recombination of carriers and the subsequent cooling of the lattice. Renormalization of the band gap is not excluded as a cause for the negative $\Delta T/T$ signal, but further analysis is needed to disentangle the different contributions. In comparison to graphene films excited at energies <0.2 μJ, an additional lifetime was required to model the growth of the negative signal in the AG films. An additional lifetime of ∼0.9 ps was extracted from the multiexponential fitting of the AG3 kinetics. This additional kinetic component is assigned to the trapping of the carriers, most probably due to the presence of oxygen in the AG films. Partial recovery of the negative $\Delta T/T$ signal in the AG films is observed, resulting in a non-decaying signal, which can be attributed to the slow recombination of trapped carriers in the >1 ns time scale. The similitude in the transient signals of AG and previously reported for graphene oxide points to the fact that the oxygen plays a major role in determining the carrier dynamics. Similarly, modeling of the ground state absorption spectra of our samples also points to the fact that oxygen is the main contributing factor. However, we cannot exclude the possibility that AG's unique morphology also contributes to both, the non-decaying signal, and to the broadened steady-state spectral features. To unambiguously differentiate the different roles played by the presence of oxygen and the unique morphology of AG films, we propose to investigate AG films with varying oxygen content. Such work is underway.

■ ASSOCIATED CONTENT

Supporting Information

The Supporting Information is available free of charge at https://pubs.acs.org/doi/10.1021/acs.jpcc.2c01086.

https://doi.org/10.1021/acs.jpcc.2c01086
J. Phys. Chem. C 2022, 126, 7949−7955

Transient change in transmission spectra of the 1 pass and 2 pass graphene and AG films and corresponding kinetics, at select wavelength, for the aforementioned samples (PDF)

AUTHOR INFORMATION

Corresponding Authors

Alexander J. Auty − *Department of Chemistry, University of Sheffield, Sheffield S3 7HF, U.K.*; Email: a.auty@sheffield.ac.uk

Adrien A. P. Chauvet − *Department of Chemistry, University of Sheffield, Sheffield S3 7HF, U.K.*; orcid.org/0000-0002-1649-0898; Email: a.chauvet@sheffield.ac.uk

Authors

Negar Mansouriboroujeni − *Department of Chemistry, University of Sheffield, Sheffield S3 7HF, U.K.*

Thiba Nagaraja − *Industrial and Manufacturing Systems Engineering, Kansas State University, Manhattan, Kansas 66506, United States*

Dimitri Chekulaev − *Department of Chemistry, University of Sheffield, Sheffield S3 7HF, U.K.*

Christopher M. Sorensen − *Department of Physics, Kansas State University, Manhattan, Kansas 66506, United States*

Suprem R. Das − *Industrial and Manufacturing Systems Engineering, Kansas State University, Manhattan, Kansas 66506, United States; Electrical and Computer Engineering, Kansas State University, Manhattan, Kansas 66506, United States;* orcid.org/0000-0003-0334-7600

Natalia Martsinovich − *Department of Chemistry, University of Sheffield, Sheffield S3 7HF, U.K.*; orcid.org/0000-0001-9226-8175

Complete contact information is available at: https://pubs.acs.org/10.1021/acs.jpcc.2c01086

Notes

The authors declare no competing financial interest.

ACKNOWLEDGMENTS

Alexander J. Auty, Adrien A. P. Chauvet, and Natalia Martsinovich are thankful to NERC (grant no. NE/T010924/1) and EPSRC (grant no. EP/R045305/1 and EP/R042802/1); S.R.D., T.N., and C.M.S. are thankful to NFS-CBET (grant no. 1935676) through the Signals in the Soil (SitS) program, and Negar Mansouriboroujeni thanks the University of Sheffield and EPSRC for her Ph.D. studentship (grant no. EP/T517835/1) to enable the present work.

REFERENCES

(1) Geim, A. K.; Novoselov, K. S. The Rise of Graphene. *Nat. Mater.* **2007**, *6*, 183−191.

(2) Avouris, P. Graphene: Electronic and Photonic Properties and Devices. *Nano Lett.* **2010**, *10*, 4285−4294.

(3) Berger, C.; Song, Z.; Li, T.; Li, X.; Ogbazghi, A. Y.; Feng, R.; Dai, Z.; Marchenkov, A. N.; Conrad, E. H.; First, P. N.; et al. Ultrathin Epitaxial Graphite: 2D Electron Gas Properties and a Route toward Graphene-Based Nanoelectronics. *J. Phys. Chem. B* **2004**, *108*, 19912−19916.

(4) Yavari, F.; Koratkar, N. Graphene-Based Chemical Sensors. *J. Phys. Chem. Lett.* **2012**, *3*, 1746−1753.

(5) Fowler, J. D.; Allen, M. J.; Tung, V. C.; Yang, Y.; Kaner, R. B.; Weiller, B. H. Practical Chemical Sensors from Chemically Derived Graphene. *ACS Nano* **2009**, *3*, 301−306.

(6) Sun, D.; Wu, Z.-K.; Divin, C.; Li, X.; Berger, C.; De Heer, W. A.; First, P. N.; Norris, T. B. Ultrafast Relaxation of Excited Dirac Fermions in Epitaxial Graphene Using Optical Differential Transmission Spectroscopy. *Phys. Rev. Lett.* **2008**, *101*, 157402.

(7) Bistritzer, R.; MacDonald, A. H. Hydrodynamic Theory of Transport in Doped Graphene. *Phys. Rev. B: Condens. Matter Mater. Phys.* **2009**, *80*, 085109.

(8) Xia, F.; Mueller, T.; Golizadeh-Mojarad, R.; Freitag, M.; Lin, Y.-m.; Tsang, J.; Perebeinos, V.; Avouris, P. Photocurrent Imaging and Efficient Photon Detection in a Graphene Transistor. *Nano Lett.* **2009**, *9*, 1039−1044.

(9) Meric, I.; Han, M. Y.; Young, A. F.; Ozyilmaz, B.; Kim, P.; Shepard, K. L. Current Saturation in Zero-Bandgap, Top-Gated Graphene Field-Effect Transistors. *Nat. Nanotechnol.* **2008**, *3*, 654−659.

(10) Dawlaty, J. M.; Shivaraman, S.; Chandrashekhar, M.; Rana, F.; Spencer, M. G. Measurement of Ultrafast Carrier Dynamics in Epitaxial Graphene. *Appl. Phys. Lett.* **2008**, *92*, 042116.

(11) Gaur, A. P. S.; Xiang, W.; Nepal, A.; Wright, J. P.; Chen, P.; Nagaraja, T.; Sigdel, S.; LaCroix, B.; Sorensen, C. M.; Das, S. R. Graphene Aerosol Gel Ink for Printing Micro-Supercapacitors. *ACS Appl. Energy Mater.* **2021**, *4*, 7632−7641.

(12) He, Q.; Das, S. R.; Garland, N. T.; Jing, D.; Hondred, J. A.; Cargill, A. A.; Ding, S.; Karunakaran, C.; Claussen, J. C. Enabling Inkjet Printed Graphene for Ion Selective Electrodes with Postprint Thermal Annealing. *ACS Appl. Mater. Interfaces* **2017**, *9*, 12719−12727.

(13) Deng, S.; Berry, V. Wrinkled, Rippled and Crumpled Graphene: An Overview of Formation Mechanism, Electronic Properties, and Applications. *Mater. Today* **2016**, *19*, 197−212.

(14) Kim, D. S.; Jeong, J. M.; Park, H. J.; Kim, Y. K.; Lee, K. G.; Choi, B. G. Highly Concentrated, Conductive, Defect-Free Graphene Ink for Screen-Printed Sensor Application. *Nano-Micro Lett.* **2021**, *13*, 87.

(15) Shang, J.; Luo, Z.; Cong, C.; Lin, J.; Yu, T.; Gurzadyan, G. G. Femtosecond UV-Pump/Visible-Probe Measurements of Carrier Dynamics in Stacked Graphene Films. *Appl. Phys. Lett.* **2010**, *97*, 163103.

(16) Chen, K.; Li, H.; Ma, L.-P.; Ren, W.; Chung, T.-F.; Cheng, H.-M.; Chen, Y. P.; Lai, T. Diversity of Ultrafast Hot-Carrier-Induced Dynamics and Striking Sub-Femtosecond Hot-Carrier Scattering Times in Graphene. *Carbon* **2014**, *72*, 402−409.

(17) Obraztsov, P. A.; Rybin, M. G.; Tyurnina, A. V.; Garnov, S. V.; Obraztsova, E. D.; Obraztsov, A. N.; Svirko, Y. P. Broadband Light-Induced Absorbance Change in Multilayer Graphene. *Nano Lett.* **2011**, *11*, 1540−1545.

(18) Gengler, R. Y. N.; Badali, D. S.; Zhang, D.; Dimos, K.; Spyrou, K.; Gournis, D.; Miller, R. J. D. Revealing the Ultrafast Process behind the Photoreduction of Graphene Oxide. *Nat. Commun.* **2013**, *4*, 2560.

(19) Rokmana, A. W.; Asriani, A.; Suhendar, H.; Triyana, K.; Kusumaatmaja, A.; Santoso, I. The Optical Properties of Thin Film Reduced Graphene Oxide/Poly (3,4 Ethylenedioxtriophene):Poly (Styrene Sulfonate)(PEDOT:PSS) Fabricated by Spin Coating. *J. Phys.: Conf. Ser.* **2018**, *1011*, 012007.

(20) Nair, R. R.; Blake, P.; Grigorenko, A. N.; Novoselov, K. S.; Booth, T. J.; Stauber, T.; Peres, N. M. R.; Geim, A. K. Fine Structure Constant Defines Visual Transparency of Graphene. *Science* **2008**, *320*, 1308.

(21) Newson, R. W.; Dean, J.; Schmidt, B.; van Driel, H. M. Ultrafast Carrier Kinetics in Exfoliated Graphene and Thin Graphite Films. *Opt. Express* **2009**, *17*, 2326.

(22) Rana, F.; George, P. A.; Strait, J. H.; Dawlaty, J.; Shivaraman, S.; Chandrashekhar, M.; Spencer, M. G. Carrier Recombination and Generation Rates for Intravalley and Intervalley Phonon Scattering in Graphene. *Phys. Rev. B: Condens. Matter Mater. Phys.* **2009**, *79*, 115447.

(23) Wang, H.; Strait, J. H.; George, P. A.; Shivaraman, S.; Shields, V. B.; Chandrashekhar, M.; Hwang, J.; Rana, F.; Spencer, M. G.; Ruiz-

Vargas, C. S.; et al. Ultrafast Relaxation Dynamics of Hot Optical Phonons in Graphene. *Appl. Phys. Lett.* **2010**, *96*, 081917.
(24) Shang, J.; Yu, T.; Lin, J.; Gurzadyan, G. G. Ultrafast Electron−Optical Phonon Scattering and Quasiparticle Lifetime in CVD-Grown Graphene. *ACS Nano* **2011**, *5*, 3278−3283.
(25) Breusing, M.; Ropers, C.; Elsaesser, T. Ultrafast Carrier Dynamics in Graphite. *Phys. Rev. Lett.* **2009**, *102*, 086809.
(26) Song, J. C. W.; Reizer, M. Y.; Levitov, L. S. Disorder-Assisted Electron-Phonon Scattering and Cooling Pathways in Graphene. *Phys. Rev. Lett.* **2012**, *109*, 106602.
(27) Alencar, T. V.; Silva, M. G.; Malard, L. M.; De Paula, A. M. Defect-Induced Supercollision Cooling of Photoexcited Carriers in Graphene. *Nano Lett.* **2014**, *14*, 5621−5624.
(28) Kaniyankandy, S.; Achary, S. N.; Rawalekar, S.; Ghosh, H. N. Ultrafast Relaxation Dynamics in Graphene Oxide: Evidence of Electron Trapping. *J. Phys. Chem. C* **2011**, *115*, 19110−19116.
(29) Styers-Barnett, D. J.; Ellison, S. P.; Mehl, B. P.; Westlake, B. C.; House, R. L.; Park, C.; Wise, K. E.; Papanikolas, J. M. Exciton Dynamics and Biexciton Formation in Single-Walled Carbon Nanotubes Studied with Femtosecond Transient Absorption Spectroscopy. *J. Phys. Chem. C* **2008**, *112*, 4507−4516.

https://doi.org/10.1021/acs.jpcc.2c01086
J. Phys. Chem. C 2022, 126, 7949−7955